Effect of wind stress forcing on ocean dynamics at air-sea interface

Hussein Yahia, Joel Sudre, Christophe Maes, Véronique Garçon

Frontiers of Information Technology & Electronic Engineering
www.jzus.zju.edu.cn; engineering.cae.cn; www.springerlink.com
ISSN 2095-9184 (print); ISSN 2095-9230 (online)
E-mail: jzus@zju.edu.cn

Effect of wind stress forcing on ocean dynamics at air sea Interface

H. Yahia[1], V. Garçon[2], J. Sudre[3], C. Maes[4]

([1]*INRIA, GEOSTAT team, Bordeaux, France, hussein.yahia@inria.fr*)

([2]*CNRS, LEGOS Laboratory, Toulouse, France, veronique.garcon@legos.obs-mip.fr*)

([3]*CNRS, LEGOS Laboratory, Toulouse, France, joel.sudre@legos.obs-mip.fr*)

([4]*Brest University, CNRS, IRD, IFREMER, LOPS, IUEM, Brest, France, christophe.maes@ird.fr*)

Received Jan. 6, 2017; Revision accepted Apr. 10, 2017; Crosschecked May 8, 2017

Abstract: In this work we evidence and study the differences in turbulence statistics in ocean dynamics carried by wind forcing at the air-sea interface. Surface currents at the air-sea interaction are of crucial importance because they transport heat from low to high latitudes. At first order, oceanic currents are generated by the balance of the Coriolis and pressure gradient forces (geostrophic current) and the balance of the Coriolis and the frictional forces dominated by wind stress (Ekman current) in the surface ocean layers. The study was conducted by computing statistical moments on the shapes of spectra computed within the framework of Microcanonical Multifractal Formalism. Remotely sensed daily datasets derived from one year of altimetry and wind data were used in this work, allowing for the computation of two kinds of vector fields: geostrophy with and geostrophy without wind stress forcing. We explore the statistical properties of singularity spectra computed from velocity norms and vorticity data, notably in relation with kurtosis information to underline the differences in the turbulent regimes associated with both kinds of velocity fields.

Key words: Ocean dynamics, remote sensing, radar altimetry, wind stress, geostrophy, Ekman currents, turbulence, multifractal formalism, wavelets, signal processing, statistical tools, singularity spectrum

1 Introduction and motivation

Due to the adequate synoptic picture of ocean circulation provided by altimetry techniques (*Chelton et al.* (2001)), refined analysis of turbulent surface ocean dynamics has become a tractable field of research. However, existing ocean circulation models which are used to compute ocean dynamics operate at spatial scales far superior to the lower limit of the ocean's inertial range. Consequently, they cannot be used presently to provide a precise quantitative analysis of the differences in turbulence statistics in both space, time (seasonal time scales) and observation scale (*Lee et al.* (2010)). A quantitative description of ocean surface turbulence statistics at different spatial and time scales finds interesting applications in oceanography. At mesoscale, geostrophic eddies dominate the turbulent motion, with radii between 10 and 100 kilometers, with notable effects on mixing, heat and climatically active tracers (*Mashayek et al.* (2017)). Submesoscale turbulence is a very active field of research, with coherent structures less than one kilometer in size down to a few meters, and a likely role in vertical mixing. Below this, the turbulent properties and characteristics of ocean dynamics close to the lower limit of the inertial range are unknown. A quantitative evaluation of the spatial and seasonal variability in the turbulent properties of ocean dynamics is a promising field of research, notably in relation with upwelling and air/sea exchanges at the interface (*Hernandez-Carrasco et al.* (2015)).

‡ Corresponding author

In this paper, we study the variations in the statistics of ocean dynamics turbulence directly from the acquired data, with a focus on mesoscale oceanic data. Our goal is to provide quantitative evaluation of wind stress forcing effects on mesoscale ocean dynamics.

2 Surface ocean dynamics

We make use of the surface ocean dynamics product at the $1/4^o$ described in (*Sudre et al.* (2013)). Our data covers one year of daily acquisitions from 2010. Using these datasets, the central hypothesis is to estimate the first order current as the sum of geostrophic and wind driven components:

- Geostrophic current is determined from the Absolute Dynamic Topography.
- Equator singularity is solved with the semi-geostrophy approximation.
- Ekman current is estimated by fitting a simple Ekman model based on the residual $\mathbf{v}_{\text{drifter}} - \mathbf{v}_{\text{geos}}$.
- Validation is performed with shipboard ADCP, equatorial moorings, SVP drifters and surface displacement Argo floats.

Using these data, we calculated the norm of geostrophic current with and without Ekman currents and the associated vorticity for the four following areas of study:

- Agulhas retroflection,
- Gulf-Stream area,
- Peru-Chile area,
- Brazil-Malvinas area .

In figure 1 we display the norm of the geostrophic surface current for the 1st January 2010. The red rectangles represent the four areas of study. For each daily acquisition from 2010 we get the norm of the oceanic velocity field with and without the Ekman currents. From these data we obtain the vorticity of the geostrophic velocity field, again with and without Ekman currents: $\omega = \nabla \wedge \mathbf{v}$.

3 Method

In the phenomenological description of turbulence, a fundamental problem is the study of the intermittency of the energy transfer *Frisch* (1995); *Parisi & Frisch* (1985); *She & Leveque* (1994); *Benzi et al.* (1984). This leads to the definition of the multifractal formalism for a quantitative and descriptive account of the breaking of self-similarity of the velocity random field $\mathbf{v}(\mathbf{x})$ at inertial range. In this formalism, intermittency is a direct consequence of the irregular geometrical structure of the repartition of energy transfer, which takes places over a spatial set of multifractal nature. In the K41 theory, at each point $\mathbf{x}$, the difference $\|\mathbf{v}(\mathbf{x}+\mathbf{r})-\mathbf{v}(\mathbf{x})\| \sim \mathbf{r}^{\mathbf{h}}\,(\mathbf{r}\to 0)$ with a same value for every $\mathbf{x}$: $\mathbf{h} = \dfrac{1}{3}$ which implies that the energy dissipation scalar field $\varepsilon(x)$ is smooth and the scaling law for the velocity random field $\Delta\mathbf{v}(\mathbf{x}, l\mathbf{r}) \doteq l^{1/3}\Delta\mathbf{v}(\mathbf{x},\mathbf{r})$ with: $\Delta\mathbf{v}(\mathbf{x},\mathbf{r}) = \mathbf{v}(\mathbf{x}+\mathbf{r}) - \mathbf{v}(\mathbf{x})$ and $\doteq$ means equality in law. Yet, the energy dissipation field is intermittent and, in fact, the scaling law occurs over a hierarchy of dense sets of multifractal nature. Moreover, the notion of a unique singularity exponent $\mathbf{h}$ must be extended and replaced by singularity exponents varying from point to point *Turiel et al.* (2008). In the canonical description of multifractality *Arneodo et al.* (1995), one considers the expectation (moment) $\mathbb{E}[\|\mathbf{v}(\mathbf{x}+\mathbf{r})-\mathbf{v}(\mathbf{x})\|^q] = \mathbb{E}[\|\Delta\mathbf{v}(\mathbf{x},\mathbf{r})\|]^q \sim \mathbf{r}^{\zeta(q)}$ with $\zeta(q)$ being a nonlinear function of the order moment q (*anomalous scaling*). If $\mathcal{F}_{\mathbf{h}}$ denotes the set of points $\mathbf{x}$ such that $\|\mathbf{v}(\mathbf{x}+\mathbf{r})-\mathbf{v}(\mathbf{x})\| \sim \mathbf{r}^{\mathbf{h}}$, then the mapping $\mathbf{h} \mapsto \mathrm{D}(\mathcal{F}_{\mathbf{h}})$ is called the singularity spectrum, with $\mathrm{D}(\mathcal{F}_{\mathbf{h}})$ being the Hausdorff dimension of the set $\mathcal{F}_{\mathbf{h}}$. The multifractal formalism can be extended outside the domain of fluid turbulence to any function or measure, or to any complex signal (*Boffetta et al.* (2002); *Turiel et al.* (2014)). From that viewpoint, the singularity spectrum previously defined appears as a particular case (the case where the signal under study is the mapping $\mathbf{x} \mapsto \|\mathbf{v}(\mathbf{x})\|$) of a more general setting available for general functions or measures, and the effective computation of singularities is achieved with wavelets. Let $\psi : \mathbb{R} \to \mathbb{R}$ a specific function called **analyzing wavelet**, $s > 0$ a strictly positive real number (the "**scale**") and $\psi_{\mathbf{s}}$

the **symmetrized scaled version** of ψ:

$$\psi_s(\mathbf{x}) = \frac{1}{\sqrt{s}}\psi\left(\frac{-\mathbf{x}}{s}\right). \quad (1)$$

Let: $\mathbf{\phi_a}(\mathbf{x}) = \mathbf{x} - \mathbf{a}$ be a translation in the signal domain and $\gamma_s(\mathbf{x}) = s\mathbf{x}$ the scale operator. The continuous wavelet transform, or CWT of a signal $\mathbf{f} \in \mathrm{L}^2(\mathbb{R})$ is the function of the two variables: $\mathbf{a} \in \mathbb{R}$ (position) and $s > 0$ (scale):

$$(\mathfrak{W}\mathbf{f})(\mathbf{a},\mathbf{s}) = \frac{1}{\sqrt{\mathbf{s}}}\left\langle\, \mathbf{f} \mid \psi \circ \gamma_{1/\mathbf{s}} \circ \mathbf{\phi_a} \,\right\rangle = \mathbf{f} * \overline{\psi_{\mathbf{s}}}(\mathbf{a}), \quad (2)$$

i.e. $\mathbf{f}$ is correlated with the two-indexed family $\frac{1}{\sqrt{s}}\,\psi \circ \gamma_{1/s} \circ \mathbf{\phi_a}$ of "**atoms**" depending on position and scale. If the analyzing wavelet has n_ψ vanishing moments, then $\mathfrak{W}\mathbf{f})(\mathbf{a}, s) \sim \mathbf{s}^{\mathbf{h(a)}}$ $s \to 0$ where $\mathbf{h}(\mathbf{a})$ is the singularity of function $\mathbf{f}$ at $\mathbf{a}$, provided $n_\psi > \mathbf{h}(\mathbf{a})$. There are many ways of computing a singularity spectrum in the canonical multifractal formalism. The most elementary, although not efficient numerically, consists in evaluating $\mathbf{h} \mapsto \mathrm{D}(\mathcal{F}_\mathbf{h})$from the CWT. Without going into detail, we mention here the basic ideas in order to get a grasp of the multifractal formalism and to introduce more sophisticated methods of computing a singularity spectrum. A "partition function" is defined with the CWT: $\mathcal{Z}(\mathbf{q}, s) = \int_{\mathbb{R}} |\mathfrak{W}\mathbf{f})(\mathbf{x}, s)|^q \mathrm{d}\mathbf{x}$. It can be shown that, in the case of multifractal signals, on has $\mathcal{Z}(\mathbf{q}, s) \sim s^{\tau(q)}$, $s \to 0$, and the singularity spectrum can be derived as a Legendre transform of $q \mapsto \tau(q)$: $\mathrm{D}_\mathbf{h} = \mathrm{D}(\mathcal{F}_\mathbf{h}) = \min_q\{q\mathbf{h} + \tau(q) + \mathrm{D}_\mathbf{f}\}$ with $\mathrm{D}_\mathbf{f}$ being a constant equal to the dimension of the support of singularities of $\mathbf{f}$. When $\tau(q)$ is smooth, one has: $q = \frac{\mathrm{dD_h}}{\mathrm{dh}}$, $\tau(q) = q\mathbf{h} - \mathrm{D}_\mathbf{h} + \mathrm{D}_\mathbf{f}$. The general shape of the singularity spectrum $\mathrm{D}_\mathbf{h}$ is given in figure 2. The left part of the spectrum is particularly interesting, as it is associated with the strongest transitions in signal $\mathbf{f}$. As we explained earlier, this method of computing a singularity spectrum is not the most accurate and it has been extended and modified in various directions: the WTMM and log-cumulant analysis method (see *Venugopal et al.* (2006) and the references herein); we will not expand upon the canonical formalism in this work, but rather turn to a micro-canonical formulation, which is able to compute alternate "spectra", based on the log-histogram approach (*Turiel et al.* (2008)), with high numerical precision and efficient algorithm. In this approach, we consider the gradient measure associated to signal f: although f is not differentiable, and, moreover, in the case of acquired data, consists of finite signals acquired at fixed spatial resolution, and we consider the data provided by ∇f computed either by finite differences or by taking the inverse Fourier Transform of $(-i\mathbf{x}\widehat{f}, -i\mathbf{y}\widehat{f})$ ($\widehat{f}$: Fourier Transform of f). The gradient measure μ is the measure on $\mathbb{R}^2$ whose density is ∇f: $\mathrm{d}\mu = \nabla f \mathrm{d}\lambda$ (λ: Lebesgue measure on $\mathbb{R}^2$). Let $\mathcal{B}_\mathbf{r}(\mathbf{x})$ the ball of radius $\mathbf{r}$ centered at point $\mathbf{x}$. Then one has:

$$\mu(\mathcal{B}_\mathbf{r}(\mathbf{x})) \;=\; \alpha(\mathbf{x})\,\mathbf{r}^{h(\mathbf{x})} \;+\; o\left(\mathbf{r}^{h(\mathbf{x})}\right)(\mathbf{r} \to 0) \quad (3)$$

with $h(\mathbf{x})$: singularity exponent of measure μ at $\mathbf{x}$. For most signals, the exponent $h(\mathbf{x})$ is independent prefactor $\alpha(\mathbf{x})$. For small scales $\mathbf{r}$ (such that the $o\left(\mathbf{r}^{h(\mathbf{x})}\right)$ term becomes negligible) the dependence on the scale parameter is concentrated in the factor $\mathbf{r}^{h(\mathbf{x})}$, and so the knowledge of the exponent $h(\mathbf{x})$ allows to interpret the type of transition which is taking place at $\mathbf{x}$. Points are classified accordingly by the "transition fronts" or "singularity manifolds" of the system. We denote by $\mathcal{F}_h$ the singularity manifold associated to the singularity value h, defined as follows (*Turiel et al.* (2008)):

$$\mathcal{F}_h \;=\; \{\mathbf{x} \;:\; h(\mathbf{x}) = h\} \quad (4)$$

As in the canonical formulation, we denote $D(h)$ the Hausdorff dimension of manifold $\mathcal{F}_h$. We retrieve in the microcanonical formalism a spectrum in the form of the mapping quantity $h \mapsto D(h)$ and the canonical exponents $\tau(p)$, associated to the structure functions of order p, are related to the spectrum $D(h)$ in the way:

$$\tau(p) \;=\; \inf_h \{ph \;+\; \mathbf{2} \;-\; D(h)\} \quad (5)$$

Conversely, if $D(h)$ is convex, the spectrum can be retrieved from the canonical exponents by applying a Legendre transform

$$D(h) \;=\; \inf_p \{ph \;+\; \mathbf{2} \;-\; \tau(p)\} \quad (6)$$

Suppose now that we evaluate the singularity at a resolution scale $\mathbf{r}_0$ which is small enough (typically the scale of the acquisition). The distribution of

singularities at this scale, $\rho_{\mathbf{r}_0}(h)$, must verify:

$$\rho_{\mathbf{r}_0}(h) \;=\; A_0\,\mathbf{r}_0^{\mathbf{2}-D(h)} \;+\; o\left(\mathbf{r}_0^{\mathbf{2}-D(h)}\right) \qquad (7)$$

Consequently, provided we know the resolution scale $\mathbf{r}_0$ we can retrieve a spectrum by just evaluating the empirical histogram of singularity exponents. We will further assume, in order to simplify the analysis, that there exists a singularity manifold $\mathcal{F}_{h_1}$ of maximum dimensionality, $D(h_1) = \mathbf{2}$. Applying such assumption to eq. (7), we obtain the following estimate of the spectrum:

$$D(h) \;=\; \mathbf{2} \;-\; \frac{\log\left(\rho_{\mathbf{r}_0}(h)/\rho^M_{\mathbf{r}_0}\right)}{\log \mathbf{r}_0} \qquad (8)$$

where $\rho^M_{r_0} = \max_h\{\rho_{r_0}(h)\}$. Eq. (8) is referred to as the "histogram method" for the evaluation of the singularity spectrum. In the rest of this article, we rely entirely on this method of computing the spectra.

4 Results

In figure 3 are shown the absolute vorticity of geostrophic and Ekman currents for the 1st January 2010 taken out of the experimentation dataset and the corresponding singularity exponents. In Figure 4 are displayed, on the left part of the image, and for the 1st January 2010 in the Agulhas retroflection area, the norm of geostrophic currents, the singularity exponents, and the associated spectrum. On the right, we show the same data for the norm of the geostrophic part and Ekman currents. The reader will notice the difference in the left part of the spectra, which is the most informative part of the spectra w.r.t. the strongest transition fronts and coherent structures, and consequently to the statistics of oceanic turbulence, as recorded in the data. That difference is quantitatively expressed by the marked difference in kurtosis between both spectra.

We now apply the methodology described in the last section on our experimental dataset, made from one year of daily data. The data used is made of altimetry and wind data, both remotely sensed (see (*Sudre et al.* (2013); *Arbic et al.* (2013)) for an in-depth description of the datasets and derived products). We compute, for each of the four areas shown in figure 1, the monthly mean kurtosis of the spectra of geostrophic norm and the monthly mean kurtosis of the singularity spectra of geostrophic vorticity. If $\mathbf{a} = (a_i)_{1\leq i\leq n}$ is a discrete signal, we use the *excess kurtosis* defined by: $\kappa = \dfrac{1}{\sigma^4}\displaystyle\sum_{i=1}^{n}\frac{(a_i - \mathbb{E}(\mathbf{a}))^4}{n}$, $\mathbb{E}(\mathbf{a})$ being the mean value of $\mathbf{a}$ and σ the standard deviation. With this definition, a standard normal distribution has a kurtosis of zero. Positive kurtosis means "heavy-tailed" distribution and negative kurtosis a "light tailed" distribution. Neat differences in kurtosis (in particular, positive and negative) mean different organizations of the multifractal hierarchy, and statistical differences in the turbulence regime. We show, in Figures 5, 6, 7 and 8, the result of the analysis for each area of study, at the monthly time scale over 2010.

5 Discussion

The results lead to the following discussion:

- Differences in kurtosis (in particular positive and negative) are significant and indicate different spectra. The norms of the velocity fields clearly show different turbulent properties between the norm of the oceanic velocity field with and without Ekman currents (*i.e.* taking into account wind stress forcing).
- We note no significant difference in term of vorticity spectra.

From these results we conclude that wind stress does affect oceanic turbulence geographically, notably w.r.t. latitude. On vorticity, it is likely that other tools than the ones presented in this work for the statistical study of turbulence have to be devised and tested.

6 Conclusion

In this article we have presented an experiment using daily, remotely sensed data acquired over one year to display different turbulence statistics of the oceanic system, with the goal of improving the description of the oceanic mesoscale (and submesoscale) turbulence. Positive results put forward the differences in term of wind stress according to the area of study. The results also confirm the usefulness of the multifractal formalism for the study of natural complex and turbulent acquired data. A turbulent regime classification for the world's oceans

is very useful to adapt the turbulent cascade pathways toward a better inference of products for super-resolution currents (*Yahia et al.* (2010); *Sudre et al.* (2013)). The methodology can also be adapted to high resolution GHG fluxes (*Hernandez-Carrasco et al.* (2015, 2018); *Garçon et al.* (2013)). The study can be extended to build a monthly climatology with the 1993-2016 period of GEKCO products for each province, and globally.

7 Figures

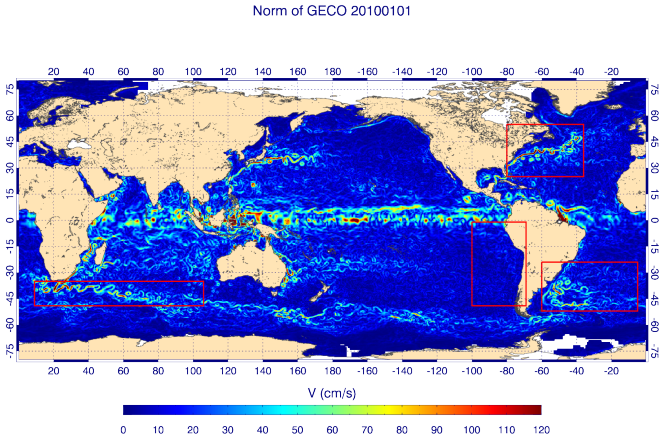

Fig. 1 Norm of the geostrophic surface current for the 1st January 2010. The red rectangles represent the four areas of study.

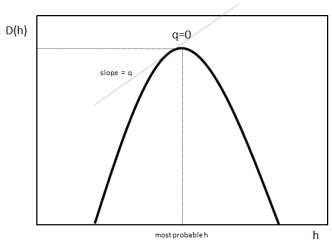

Fig. 2 General shape of the singularity spectrum $\mathrm{h} \mapsto \mathrm{D_h}$ as the Legendre transform of $q \mapsto \tau(q)$.

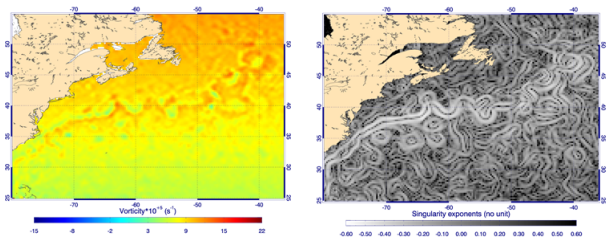

Fig. 3 Left: absolute vorticity of geostrophic and Ekman currents for the 1st January 2010. Right: Corresponding singularity exponents.

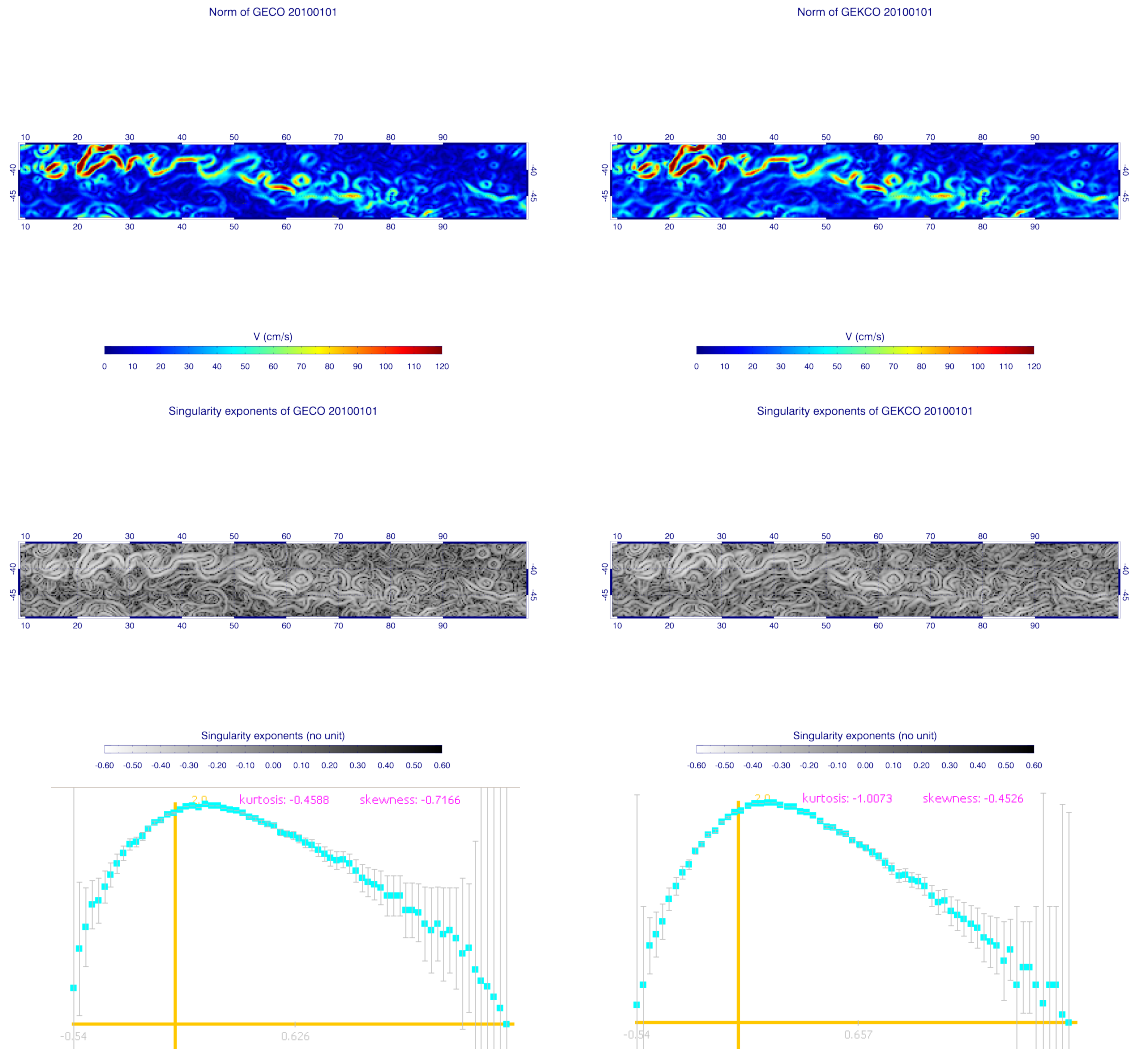

Fig. 4 Left (top to bottom): for the 1st January 2010 in the Agulhas area, norm of geostrophic currents (top), singularity exponents (middle), associated spectrum (bottom). Right (top to bottom): for the 1st January 2010 in the Agulhas area, norm of geostrophic and Ekman currents (top), singularity exponents (middle), associated spectrum (bottom). Error bars in the spectra are computed using the method described in *Turiel et al.* (2006).

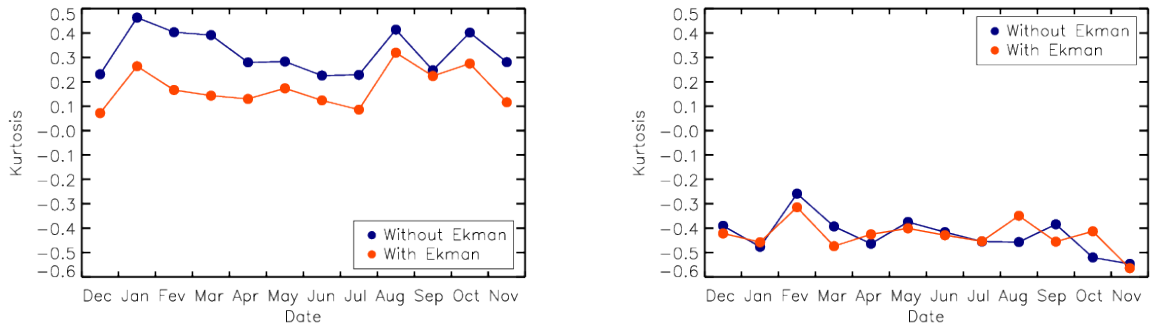

Fig. 5 Results: Gulf Stream area. Left: monthly mean kurtosis of the spectra of geostrophic norm. Right: monthly mean kurtosis of the spectra of geostrophic vorticity.

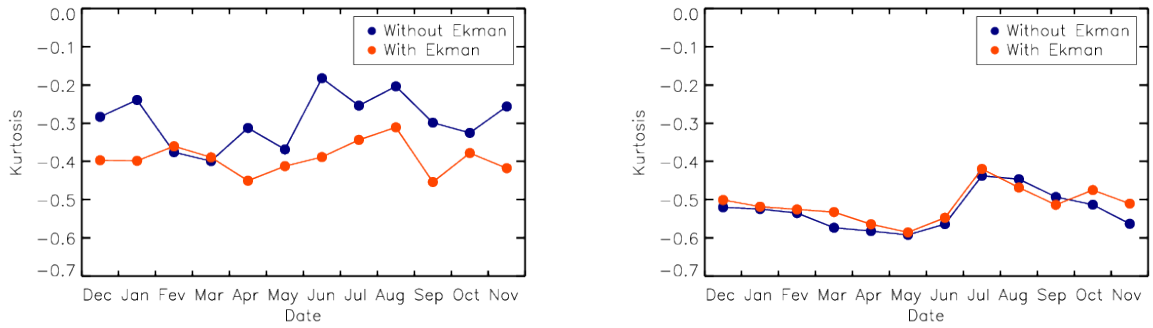

Fig. 6 Results: Brazil-Malvinas area. Left: monthly mean kurtosis of the spectra of geostrophic norm. Right: monthly mean kurtosis of the spectra of geostrophic vorticity.

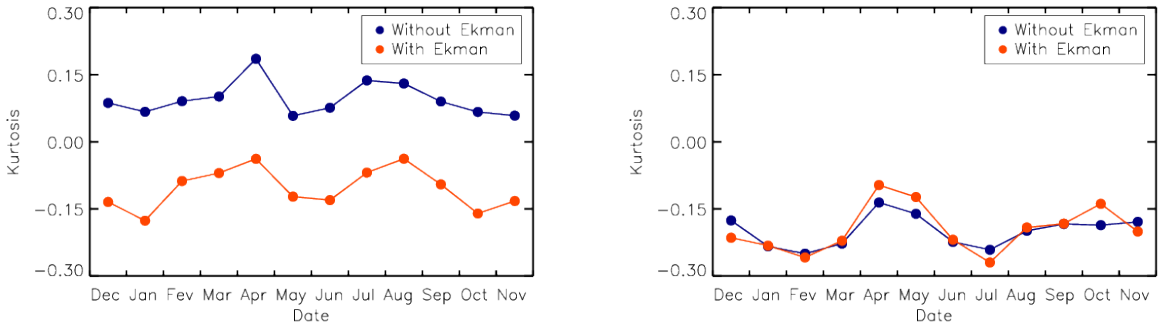

Fig. 7 Results: Agulhas area. Left: monthly mean kurtosis of the spectra of geostrophic norm. Right: monthly mean kurtosis of the spectra of geostrophic vorticity.

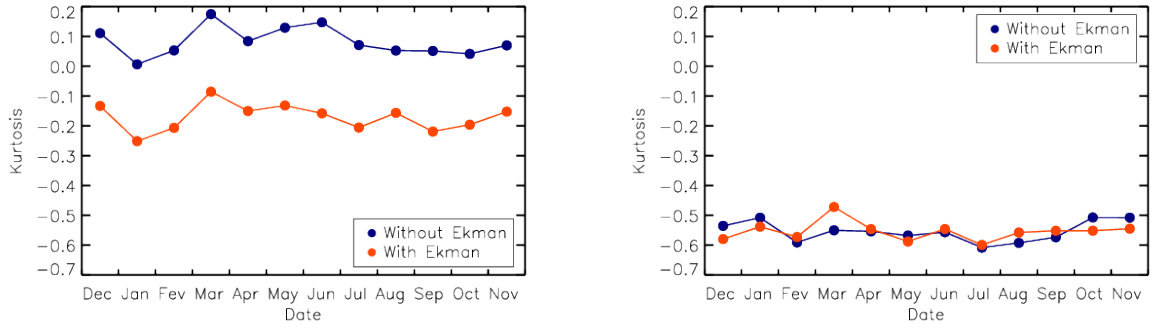

Fig. 8 Results: Peru-Chile area. Left: monthly mean kurtosis of the spectra of geostrophic norm. Right: monthly mean kurtosis of the spectra of geostrophic vorticity.

REFERENCES

Arbic, B. K., K. L. Polzin, R. B. Scott, J. G. Richman and J. F. Shriver, (2013), On Eddy Viscosity, Energy Cascades, and the Horizontal Resolution of Gridded Satellite Altimeter Products, *Journal of Physical Oceanography,43*, doi:10.1175/JPO-D-11-0240.1, 283–300.

Arneodo, A., E. Bacry, and J. F. Muzy, (1995), The thermodynamics of fractals revisited with wavelets, *PhysicaA,213*, 232–275.

Benzi, R., G. Paladin, G. Parisi and A. Vulpiani (1984), On the multifractal nature of fully developed turbulence and chaotic systems, *J. Phys. A: Math. Gen,17*, 3521–3531.

Boffetta, G., M. Cencini, M. Falcioni and A. Vulpiani, (2002), Predictability: a way to characterize complexity, *Physics Reports 356*, 367–474, ArXiv ID: nlin.CD/0101029, doi: 10.1016/S0370-1573(01)00025-4.

Chelton, D. B., J. Ries, B. Haines, L.-L. Fu and P. Callahan, (2001), in Satellite Altimetry and Earth Sciences: A Handbook of Techniques and Applications, *International geophysics series*,(Lee-Lueng Fu, Anny Cazenave Eds.) *69*, 1–122.

Frisch, U., (1995), *Turbulence: The Legacy of A. N. Kolmogorov*, Cambridge University Press, ISBN 0-521-45713-0 (pb), 1995.

Garçon, V., et al. (2013), Perspectives and integration, in Ocean-Atmosphere Interactions of Gases and Particles, *SOLAS Science* (Liss, P. S. and Johnson, M. T.), *Springer*, 247–306.

Hernandez-Carrasco I., J. Sudre, V. Garçon, H. Yahia et al., (2015), Reconstruction of super-resolution ocean pCO_2 and air sea fluxes of CO_2 from satellite imagery in the southeastern Atlantic, *Biogeosciences*, doi:10.5194/bg-12-5229-2015.

Hernandez-Carrasco I., V. Garçon, J. Sudre, C. Garbe, H. Yahia, (2015), Increasing the Resolution of Ocean pCO_2 Maps in the South Eastern Atlantic Ocean Merging Multifractal Satellite-Derived Ocean Variables, *IEEE Transactions on Geoscience and Remote Sensing*, doi: 10.1109/TGRS.2018.2840526.

Lee, N. J. P. L. et al., (2010), Ocean State Estimation for Climate Research, *Proceedings of OceanObs 09: Sustained Ocean Observations and Information for Society (Vol. 2)*, (Hall, J., Harrison, D.E. & Stammer, D., Eds.) *ESA Publication WPP-306*, doi: 10.5270/OceanObs09.cwp.55, 643–651.

Mashayek A., R. Ferrari, S. Merrifield, J. R. Ledwell, L. St Laurent A. Naveira Garabato, (2017), Topographic enhancement of vertical turbulent mixing in the Southern Ocean *Nature Comm.*, doi: 10.1038/ncomms14197.

Parisi, G. and Frisch, U., (1985), On the singularity structure of fully developped turbulence, in Turbulence and Predictability in Geophysical Fluid Dynamics, Proc. Intern. School of Physics 'E. Fermi, *North Holland*, (M. Ghil, R. Benzi & G. Parisi Eds.), 84–87.

She, Z.-S. and F. Leveque, (1994), Universal scaling laws in fully developed turbulence, *Physical Review Letters,72*(3), doi:10.1103/PhysRevLett.72.336, 336–339.

Sudre, J., C. Maes, V. Garçon, (2013), On the global estimates of geostrophic and Ekman surface currents, *Limnology & Oceanography: Fluids & Environments,3*, doi:10.1215/21573689-2071927, 1–20.

Thomas, L. N., A. Tandon and A. Mahadevan, (2008), in Ocean Modeling in an Eddying Regime, Geophysical Monograph Series, *American Geophysical Union, Washington, D. C.*,(M. W. Hecht, H. Hasumi, Eds.) *177*, 17–38.

Turiel A., C. J. Pérez-Vicente and J. Grazzini, (2006), Numerical methods for the estimation of multifractal singularity spectra on sampled data: A comparative study, *Journal of Computational Physics*, *216*(1), 362–390.

Turiel, A., H. Yahia and C. J. Pérez-Vicente (2008), Microcanonical multifractal formalism – a geometrical approach to multifractal systems: Part I. Singularity analysis, *J. Phys. A: Math. Theor.,41*(015501), doi:10.1103/PhysRevE.74.061110.

Turiel, A., J. Isern-Fontanet and M. Umbert (2014), Sensibility to noise of new multifractal fusion methods for ocean variables, *Nonlin. Processes Geophys.*, *21*, 291–301, doi:10.5194/npg-21-291-2014.

Venugopal, V., S. G. Rous, E. Foufoula-Georgiou and A. Arneodo (2006), Revisiting multifractality of high-resolution temporal rainfall using a wavelet-based formalism, *Water Resources Research*, *42*, doi:10.1029/2005WR004489.

Yahia, H., J. Sudre, C. Pottier, V. Garçon, (2010), Motion analysis in oceanographic images sequences using multiscale methods and the energy cascade, *Pattern Recognition,43*(10), doi:10.1016/j.patcog.2010.04.011, 3951–3604.